# MELCOR Integrated Severe Accident Code Application to Safety Assessment of Heat Pipe Reactors

K.C. Wagner,\* C. Faucet,† R. Schmidt, L.L. Humphries,‡ and D.L. Luxat§

\*Sandia National Laboratories, New Mexico, P.O. Box 5800, Albuquerque, NM 87185, kcwagne@sandia.gov †Sandia National Laboratories, New Mexico, P.O. Box 5800, Albuquerque, NM 87185, cfaucet@sandia.gov \*Sandia National Laboratories, New Mexico, P.O. Box 5800, Albuquerque, NM 87185, rschmi@sandia.gov \*Sandia National Laboratories, New Mexico, P.O. Box 5800, Albuquerque, NM 87185, llhumph@sandia.gov \*Sandia National Laboratories, New Mexico, P.O. Box 5800, Albuquerque, NM 87185, dlluxat@sandia.gov

[leave space for DOI, which will be inserted by ANS]

### INTRODUCTION

MELCOR is an integrated systems-level severe accident code used for source term analysis [1][2]. It has been developed at Sandia National Laboratories for the United States Nuclear Regulatory Commission since the early 1980s. Current MELCOR development efforts have been focused on providing the U.S. NRC (NRC) with the analytical capabilities to support regulatory readiness for licensing nonlight water reactor (LWR) technologies under Strategy 2 of the NRC's near-term Implementation Action Plans [3]. MELCOR has recently undergone a range of enhancements to provide analytical capabilities for modeling the spectrum of advanced non-LWR concepts. In this paper, we describe the generic MELCOR plant model developed to demonstrate MELCOR capabilities to perform heat pipe reactor (HPR) safety evaluations.

The HPR has hexagonal uranium dioxide (UO<sub>2</sub>) fuel assemblies surrounding a heat pipe (HP). The heat pipes transfer heat from the core to the heat exchanger above the core that is part of an open-air Brayton cycle. Surrounding the reactor vessel is a reactor cavity that is located at the bottom of the confinement building. The reactor is passively cooled by the natural convection flow within the reactor cavity and confinement building. A range of demonstration calculations are performed to evaluate MELCOR's capabilities to characterize the HPR response for a range of scenarios. The accidents selected for evaluation consider a range of degraded and failed modes of operation for key safety functions providing reactivity control, primary system heat removal and reactor vessel decay heat removal.

## 1. MELCOR HTGR Modeling Features

The MELCOR code is organized into "packages" that correspond to different groupings of reactor regions, physics, or other code functionalities. The balance of the plant is modeled using the building block components of control volumes, heat structures, and flow paths. These basic components are used to represent primary system, the reactor vessel, the reactor building or containment, and the secondary system, which will be described for the HPR demo model in the next section. These fundamental modeling features are

universally used for all reactor types and non-reactor buildings. The unique capability of MELCOR includes an integrated calculation of radionuclide release, transport, and deposition in any problem description or nodalization.

A HPR works based on transferring the latent heat of vaporization of a working fluid from the evaporator region to condenser region. The nuclear heat source evaporates the working fluid in the wick of the HP. The gas flows to the condenser down the interior of the heat pipe based on the pressure gradient formed by gas generation in the evaporator at one end and gas condensation at the other end. The heat transfer from the HP wall to the secondary fluid condenses the gas on the wick adjacent to the HP wall. The liquid flows back to the evaporator along the wick due to the capillary forces created by the gas-phase pressure gradient in the center of the HP. The HP was created and demonstrated at LANL and has seen applications for space power system, domestic heating, and as a demonstration HPR [4].

The level of modeling detail or discretization is user-specified based on the objectives of the analysis. An example for the Los Alamos National Laboratory (LANL) Megapower HPR [5] as modified in the Idaho National Laboratory (INL) Design A reactor description [6] is presented in this paper. The next subsections describe some of the key MELCOR models used in the HPR demo calculations and an overview of the calculation solution methodology.

## 1.1 MELCOR HPR Model

Superimposed in the reactor core portion of the vessel nodalization is a special model for HP modeling. The HP geometry description and associated physics are modeled in the "COR" package. The HP COR modeling includes representation of the HP wall, the fuel and the interface between the fuel and the HP, the HP working fluid, the HP connection to the secondary heat exchanger, the HP performance limitations, and various HP failure modes [2].

Fig. 1 illustrates key aspects and regions of a vertically oriented generic HP. A MELCOR HP model is specified by the key geometric attributes, which include the HP radius, the HP wall thickness, the interior wick thickness, and the porosity of the wick.

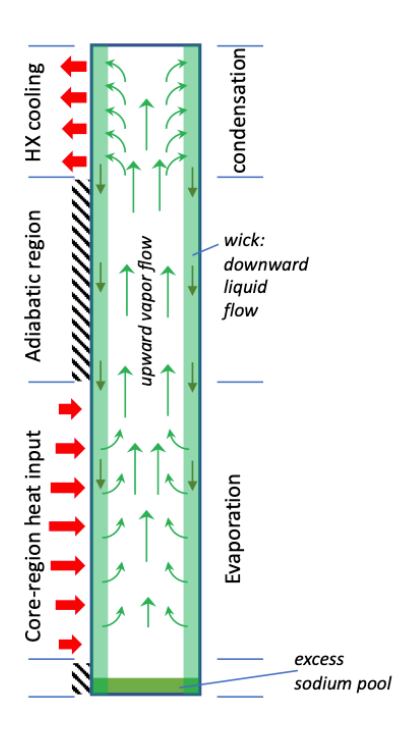


Fig. 1. Illustration of a vertically oriented heat pipe.

The HP is subdivided into three sections, (1) the evaporator region, (2) the adiabatic region, and (3) the condenser region. Each of these HP sections are implicitly connected to specified COR package cells. Consequently, the COR nodalization for a HPR includes the active fuel region, the adiabatic region, and the condenser region. In addition, the HPR COR model includes the lower vessel head and any plenum region below the core. The HP model includes multiplicity scaling of a representative HP in the specified COR region, separate instances of HP models in other COR regions to support a discretized radial nodalization, and provisions for alternate geometry or performance criteria with multiple types of HP models. The HP model supports either sodium or potassium as the working fluid.

The fuel adjacent to or surrounding the HPs is modeled with the fuel component. The interface between the heat pipe and the fuel is modeled with a heat conductance pathway between the fuel and the HP wall. The heat transfer connection to the condenser region connection is modeled between the HP wall and the fluid in the secondary side of the HP. In the adiabatic region, the model assumes no heat transfer from/to the HP outer wall.

The MELCOR HP model assumes that the working fluid is in thermodynamic equilibrium. The equilibrium state is dynamically calculated based on based on the mass, volume, and enthalpy of the working-fluid in the HP. The enthalpy is used to calculate the HP pressure, temperature, and quality. The required thermodynamic properties of the working fluid (i.e., sodium or potassium) were added as part of the model development. Reference [2] provides a detailed description of the governing equations and numerical implementation.

HPs have performance limitations that can be characterized in steady state codes such as LANL's HTPIPE code [7]. There are a variety of operational limits that can constrain the performance of the heat pipe. Details of these constraints are described in the HP literature (e.g., see References [6][7][8]). The MELCOR HP model includes consideration of sonic, capillary, and boiling limits. The sonic limit is associated with choked flow of vapor through the central core. The capillary flow limit concerns the maximum liquid flow through the wick. The boiling limit concerns the onset of nucleate boiling within the evaporator section wick that degrades the heat transfer efficiency.

An example of the HP performance limits from the INL Design A HPR description report is shown in Fig. 2. It includes the sonic, entrainment, capillary, and boiling limits. The entrainment limit concerns liquid entrainment off the wick due to high vapor velocities, which is not more limiting than the gas phase sonic limit in this example. The HP performance limits are highly dependent on the HP geometry and the wick construction, the HP orientation, and the working fluid. The operating power versus fluid temperature shown in Fig. 2 is the typical presentation of the limits.

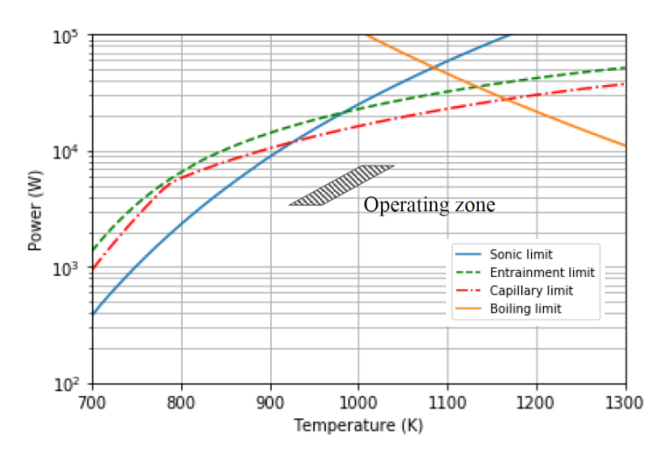


Fig. 2. Example HP operational limits [6].

## 1.2 MELCOR HP Failure Models

The MELCOR HP model includes several failure modes. For example, the vapor flow to the condenser is limited by the sonic limit and the liquid flow returning to the evaporator section is limited to the capillary limit. The three most important failure modes for the HPR demo calculations are the boiling limit, HP wall failure due to melting, and HP wall failure due creep rupture. Each of these failure modes will be discussed next.

The boiling limit is implemented as a maximum local heat flux in a COR cell. The boiling heat limit from a performance curve such as Fig. 2 is converted to a maximum flux, which is compared to the local COR cell heat flux. If the maximum boiling flux is exceeded, then the heat transfer coefficient between the working fluid and the heat pipe wall

degraded. The boiling limit does not directly fail the HP but will typically lead to a rapid rise in the local heat pipe wall temperature.

The second mode of HP failure, which follows the boiling limit in the HPR demonstration calculation, is a melting failure of the HP wall. The INL Design A HP uses a stainless steel cladding around the fuel and a stainless steel HP wall. The MELCOR model assumes the fuel cladding and HP wall fail simultaneously near the melting temperature of stainless steel. The heat pipe is at high pressure and temperature and expected to yield as the adjacent fuel cladding temperature approaches the stainless steel melting point (i.e., assumed to occur at 1650 K in the demonstration calculation). When the HP wall fails, the high pressure fluid exits from the HP and it ceases to operate.

A third failure mode is creep rupture of the HP wall. At high power conditions, the pressure and temperature of the fluid in the HP increases. As shown in Fig. 3, the pressure rapidly rises from the normal subatmospheric condition to high pressure as the HP temperature increases above 800°C. At high pressures and temperatures, the HP wall will strain and fail. In addition to a melting failure in the core region, a creep rupture failure due to creep at the top of the core or in the condenser is evaluated using the built-in Larson-Miller lifetime failure model for stainless steel pipes [2]. If the creep rupture criteria is exceeded, then the wall of the HP fails. Similar to the local melting failure in the core, the high pressure fluid exits from the HP and it ceases to operate.

Fig. 4 shows the HP and the fuel cladding failure locations described above. The fuel cladding failures are particularly important because this begins the start of the fission product release from the fuel. The upper two HP failures are illustrative of creep ruptures at high pressure and temperature. Since the fluid in the HP is approximately isothermal (i.e., also an assumption in the MELCOR model), a creep failure can occur almost anywhere along the HP wall. However, it should be noted that the pipe wall stress in the condenser is different than the core due to different pressures on the pipe wall. Weld and flaw locations would be more especially vulnerable but also difficult to characterize. Once the pipe fails and depressurizes, an additional creep rupture failure is not possible.

Finally, the movement of a HP on a performance limit chart such as Fig. 2 is controlled by the heat removal characteristics of the secondary system. The temperature rise associated with an increase in power, or vice versa, depends on the secondary response to the higher heat load. If the flow and inlet temperature are steady, then the HP temperature rise is controlled by the secondary fluid temperature rise (and any changes in the heat transfer coefficient). The operational grid in Fig. 2 illustrates this primary to secondary energy balance limit.

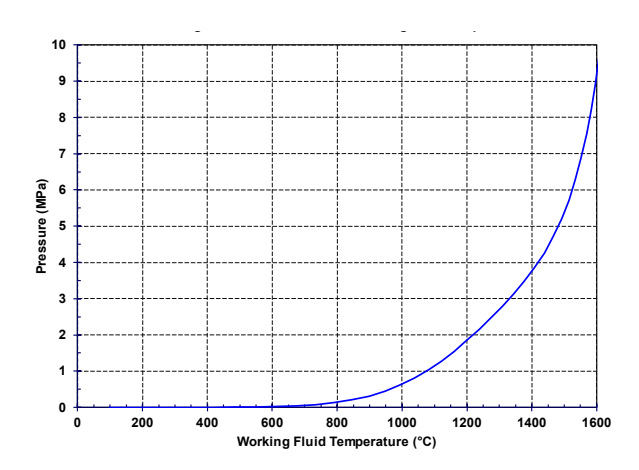


Fig. 3. Potassium Equilibrium Pressure Temperature Curve.

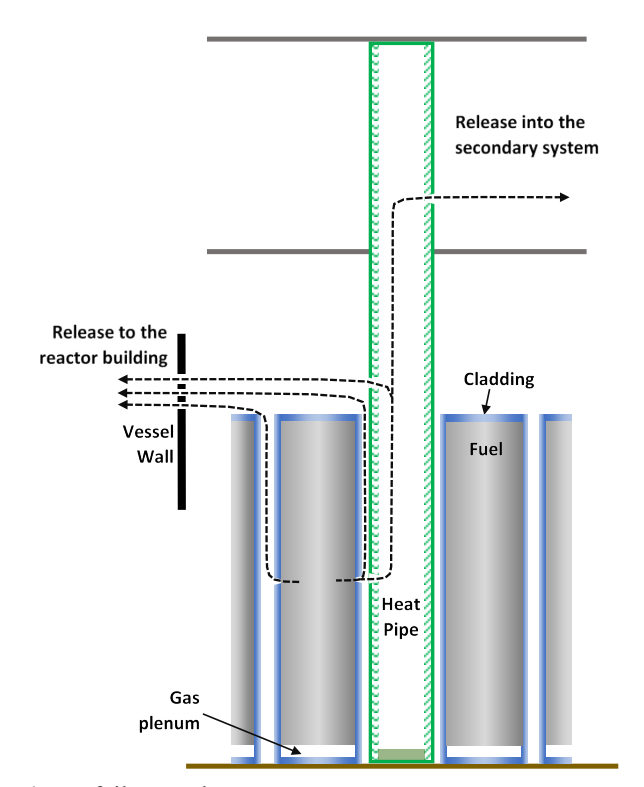


Fig. 4. HP failure pathways.

# 2. The INL Design A HPR Demonstration Model

The scope of the INL design report analysis did not include all the components required for a mechanistic source term (MST) evaluation. The vessel and core of the INL Design A heat pipe model was constructed using information primarily documented in the INL design report [6]. The report provided geometric and analysis details for most of the required input. The HP system performance limits were developed using the LANL HTPIPE code [7], which allowed specification of the specific geometry of the INL Design A HP. The INL design report did not include information on the secondary system, which was supplemented using INL

conference presentation material [9]. The LANL and INL design reports did not include information about the surrounding reactor building. The inputs for the reactor building were estimated based on experience with the boiling water reactor (BWR) enclosure building. The radionuclide inventory and decay heat tables were obtained from a supporting SCALE analysis by Oak Ridge National Laboratory (ORNL). ORNL also provided the axial and radial power profiles and reactivity feedbacks.

## 2.1 INL Design A HPR Overview

A cross-section of the INL Design A reactor vessel is shown in Fig. 5 and the reactor vessel and secondary system schematic is shown in Fig. 6 (i.e., except the reactor vessel and internal heat pipes are vertical rather than horizontal). The key design features are summarized in Table 1. The core is formed in a hexagonal shape with a circular center for the emergency control rods. 1134 hexagonal fuel assemblies are arranged around the hexagonal core. The core is surrounded by a large 19.4-27.3 cm alumina reflector that contains 12 control drums for reactivity control. The control drums can slowly turn the B<sub>4</sub>C arcs to increase or decrease reactivity. The alumina reflector is surrounded by a 5.1 cm stainless steel core barrel assembly and a 15.2 cm B<sub>4</sub>C radiation shield. There are beryllium oxide reflectors above and below the core.

The active fuel region is 150 cm. The fuel is a 19.75 wt% high-assay, low-enriched uranium (HALEU) with a maximum burn-up of 2 GWD/MTU. The mass of the <sup>235</sup>U is 904 kg. The expected design life is 5 years.

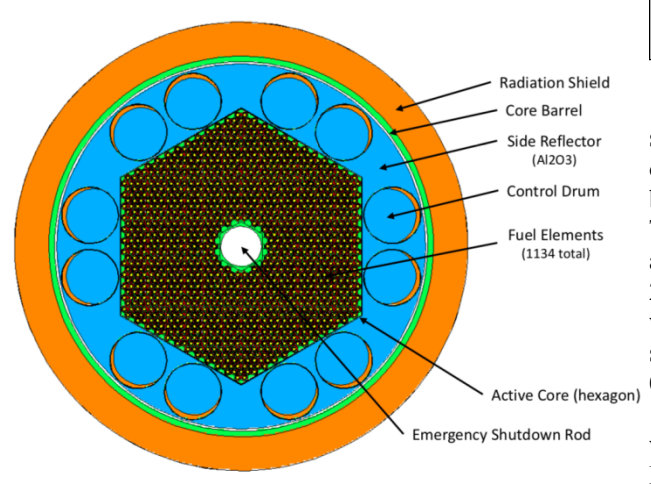


Fig. 5. INL Design A reactor vessel cross-section [6].

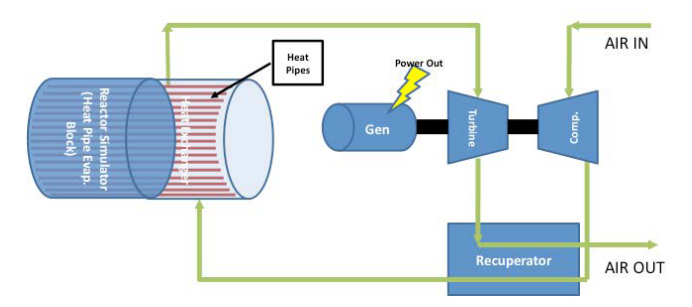


Fig. 6. INL Design A reactor and secondary design schematic [9].

Table 1. Key Parameters for the INL Design A HPR [6].

Parameter	Value
Reactor thermal power	5 MW
Fuel elements	1134 hex elements 5.2 MT of UO <sub>2</sub> 19.75 wt% enrichment
HPs	1134 HPs with potassium working fluid
Reactivity control	12 alumina control drums with arcs of B <sub>4</sub> C for reactivity control
Shutdown system	2 B <sub>4</sub> C emergency control rods
Secondary system	Brayton open-air power cycle

A cross-section of the INL Design A HP fuel element is shown in Fig. 7. The circular heat pipe is located in the center of each fuel element. There are very small gaps (0.0064 cm) between HP and the fuel assembly stainless steel cladding. There are also small gaps between the hexagonal fuel element and the inner and outer cladding. The fuel element pitch is 2.7862 cm. The HP outer diameter is 1.757 cm with a 0.1 cm wall thickness. The heat pipe is 4 m long with a 1.5 m segment in the condenser region. The adiabatic length is 0.4 m. The average heat pipe power is 4.41 kW.

The INL Design A heat pipe performance limit curves were generated using LANL HTPIPE code [7] with the INL Design A geometry and a potassium working fluid. The curves generated by the HTPIPE code (see Fig. 8).

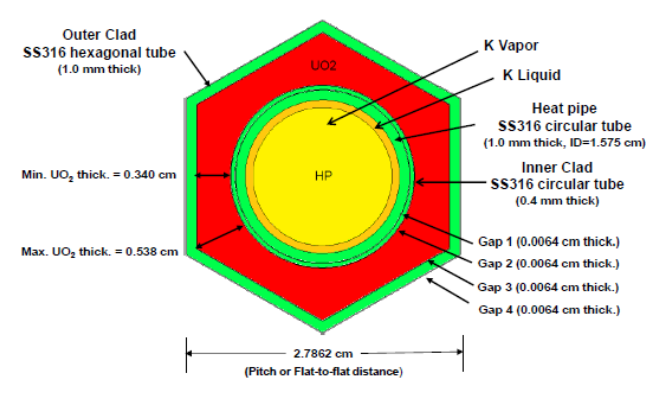


Fig. 7. INL Design A HP and fuel element cross-section [6].

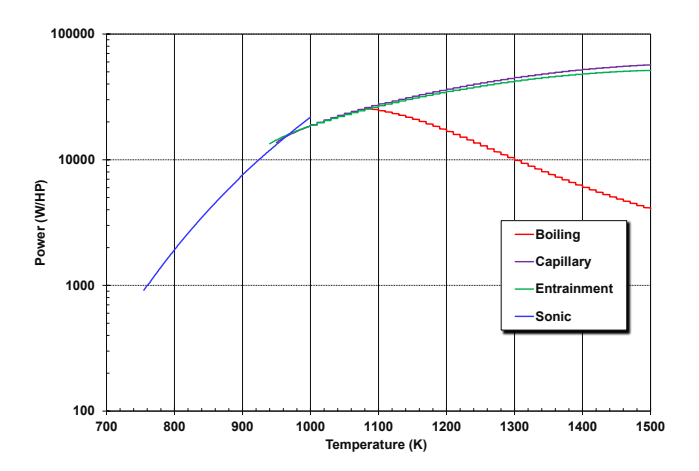


Fig. 8. INL Design A HP limit curves.

# 2.2 Reactor Vessel Nodalization

The modeling of the INL Design A reactor vessel in MELCOR utilizes building block inputs from multiple packages. The building block approach to the input gives lots of flexibility to model alternate reactor designs with varying levels of resolution. A key set of vessel input comes from COR Package, which includes structures in the core and the radionuclide release model. The INL Design A COR nodalization has 14 axial levels and 15 radial rings, which are in cylindrical coordinates (see Fig. 9). The COR package includes (a) the active core region with the evaporation section of the HPs (i.e., the region within axials levels 3-12 and rings 2-15), (b) the center, top and bottom reflectors surrounding the core, (c) the HP extension through the adiabatic region (axial level 13) and the condenser region (axial level 14), the core baffle surrounding the hexagonal core (also in ring 15), and (e) the region below the active core that includes bottom reflector and the fuel gas plenum in axial levels 1-2. The large alumina side reflectors, the core barrel, and the B<sub>4</sub>C radiation shield are modeled in the heat structure (HS) package but thermally coupled to the COR region. There is equal spacing between the radial rings in the active core (rings 2-15) that corresponds to the width of a fuel element (28 cm). There are 10 equally spaced (15 cm) axial levels in the active core.

Each COR ring includes a separate HP model that corresponds to the number of HPs within the ring radii. The HPs are assumed to respond identically within a COR ring. However, MELCOR includes the flexibility to have HPs with alternate characteristics (e.g., the limit or failure criteria) within the same ring. Each HP becomes a normal fluid control volume (CV) upon its failure. The CVs track the pressure and temperature in the HP and depressurize into the vessel or the secondary upon their failure. There provisions for a heat pipe wall melting failure and creep failures in the vessel and condenser for each of the 14 rings with HPs in the core. The failures are modeled with flow paths connected to the appropriate failure signals.

A single control volume is used to represent the interstitial regions around the fuel elements. A CV represents the secondary side of the condenser with flow path connections for the upstream and downstream boundary secondary boundary conditions. The secondary is assumed to blowdown to the atmosphere when the secondary recirculation fan trips off. The interstitial regions in lower plenum are also modeled with a separate CV. There is a variable sized leakage path from the adiabatic region to the reactor building where released radionuclides can leak out (see Fig. 4). An uncertainty study examined the importance of the vessel leakage area on the system response and the magnitude source term (i.e., not presented here).

The COR package models the heat transfer and physics routines for the materials in the core, any material relocation, the eutectic interactions, the support structure degradation, and the lower reactor head heatup and failure. The demo calculation included melting and relocation of some stainless steel cladding material but no gross relocation of the fuel elements.

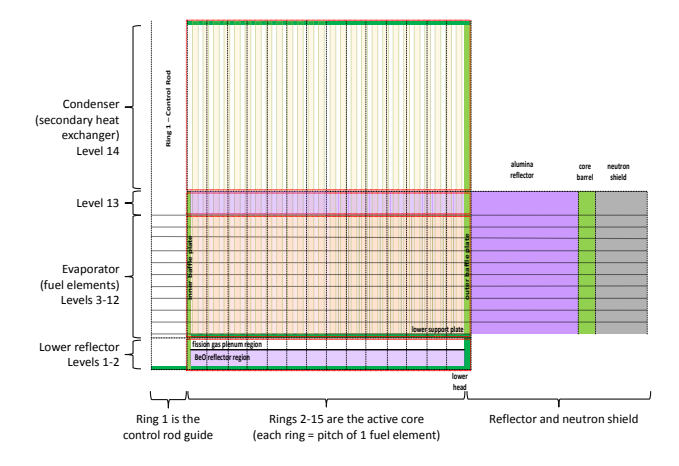


Fig. 9. INL Design A reactor vessel nodalization.

## 2.3 Reactor Building Nodalization

For the demonstration calculations, a reactor building was developed based on a concept of a BWR reactor building

surrounding a BWR/4 Mark I containment. The INL Design A report indicated that the reactor should be placed in a concrete reactor cavity for additional shielding protection. It is expected the reactor would be below grade with a surrounding building that includes below-grade and above grade rooms as shown in Fig. 10. The first floor around the reactor would have limited access with the turbine, compressor, and recuperator located on the second floor (see Fig. 6).

The circular reactor cavity had 191 m<sup>3</sup> of gas space surrounding the reactor. The reactor building dimensions were specified to 464 m<sup>2</sup> distributed between two floors. Each floor is 4.575 m high for a total below- and above-grade height of 9.15 m.

The reactor cavity, the first floor, and the second floor were modeled with separate CVs. There are two flow paths between each region to facilitate natural circulation. The reactor cavity flow areas were estimated based on the open space between the vessel and cavity wall. The flow paths between the first and second floor of the reactor building are modeled as the area of two stairwells.

The building leakage was scaled similar to a BWR reactor building (i.e., 100% leakage per day at a design pressure of 0.25 psi). When there is an external wind, one flow path is assigned to the upwind side of the building and the other is on the downwind side.

The wall thicknesses were selected to ensure that the reactor building maintains a three hour fire rating in accordance to typical nuclear fire protection programs. Currently the reactor building is only split up into two distinct areas, the first and second floor. This is a simplification and additional walls and rooms are expected.

The purpose of the cavity wall is for radiation shielding but also acts as a large heat sink to absorb the radiative heating from the vessel. The heat capacity of the cavity wall is important in scenarios where the reactor vessel overheats.

### 2.4 Radionuclide Inventory

The radionuclide inventory and decay heat input was calculated using SCALE by Oak Ridge National Laboratory (ORNL) [10]. The nuclides from the SCALE calculation are grouped and assigned to one of the twelve MELCOR radionuclide classes. The 5-year end-of-cycle burn-up results were used for the demonstration calculations, which was approximately 2 GWd/MTU. The data provided from SCALE includes separate decay heat curves for each of MELCOR's radionuclide classes [1]. Table 2 shows the radionuclide inventory from the SCALE analysis and MELCOR's 12 radionuclide groups, although additional radionuclide groups are subsequently introduced to model chemical compounds of cesium and iodine.

The axial and radial power profiles were also provided by ORNL using SCALE. The axial profile is approximately cosine-shaped with a maximum axial peaking factor of 1.25. The top and bottom of the axial power profile have strong peaks (i.e., 1.04 at the bottom and 0.79 at the top) due the beryllium reflectors. The radial power is skewed toward the center with a maximum of 1.4 at the fuel assemblies closest to the center.

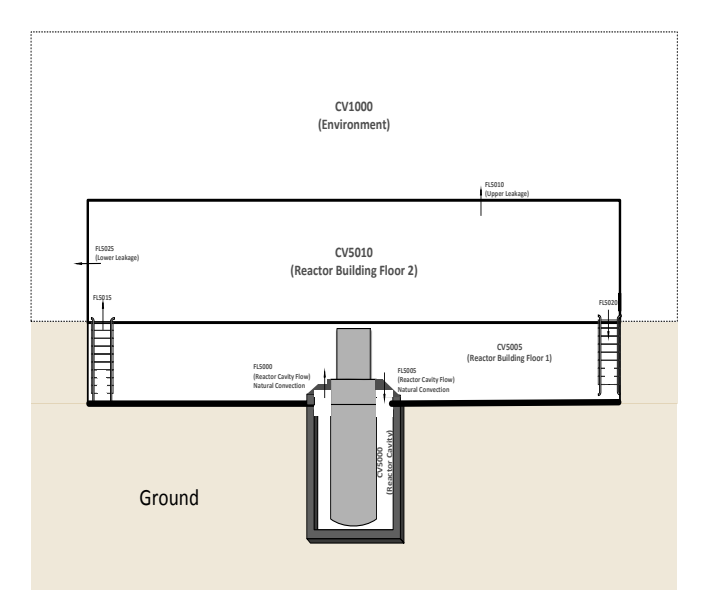


Fig. 10. HPR reactor building nodalization.

Table 2 INL Design A Radionuclide Inventory.

MELCOR RN class	Mass (kg)
Noble Gases (Xe)	1.326
Alkali Metals (Cs)	1.187
Alkaline Earths (Ba)	0.723
Halogens (I)	5.28e-2
Chalcogens (Te)	0.139
Platinoids (Ru)	0.761
Early Transition Elements (Mo)	1.229
Tetravalent (Ce)	6.770
Trivalents (La)	2.291
Uranium (U)	4565.4
More Volatile Main Group (Cd)	1.08e-2
Less Volatile Main Group (Ag)	3.9e-3

### 2.5 Radionuclide Release Input

The MELCOR fuel behavior release model calculates the release of radionuclides from the fuel elements. The light water reactor CORSOR-Booth model is used to predict the radionuclide release, which has been benchmarked to available LWR fuel release data [11]. The low-burnup CORSOR-Booth model was selected. However, the INL Design A burn-up is very low. The impact was judged to be small relative to other uncertainties.

### 2.6 Point Kinetics Modeling

MELCOR includes a fast-running, six-group point kinetics model for the dynamic simulation of the reactor power. The INL Design A reactivity feedbacks were calculated by ORNL from their full-core, 3-dimensional, continuous energy simulations. The results were in good agreement with the INL design report. The ORNL analysis included the radial expansion effects of the stainless steel clad, the gap closure and increased pitch, the alumina radial expansion, and the control drum drift. The calculated feedback coefficients are shown in Table 3.

Table 3 INL Design A Feedback Coefficients.

Feedback Effect (cents/°C)	SCALE
Doppler	-0.1113
UO <sub>2</sub> Fuel Axial Elongation	-0.0437
Alumina Reflector Radial Thermal Expansion	-0.0284
All Radial Expansions (Clad, Reflector, and CDs)	-0.0636
Total	-0.2185

The reactivity feedbacks shown in Table 3 illustrate important inherent safety features of the INL Design A HPR. The system has a very strong negative reactivity response to a temperature rise. Consequently, in an overheating accident, the reactor fission reaction will naturally shutdown as the temperature rises, especially due to expansion effects. Conversely, the reactivity will increase as the reactor cools which provides a degree of inherent control during normal operations. The operators (or the control system) will make small adjustments to the control drum rotational position for normal power operations.

ORNL also reported the total drum worth as \$11.38 and the annular and solid emergency control rod worth as \$11.75 and \$9.70, respectively.

### DISCUSSION AND EXAMPLE RESULTS

The INL Design A HPR input model was used to demonstrate MELCOR's mechanistic HPR mechanistic source term capabilities. A transient over-power (TOP) sequence was selected after reviewing the results from the loss-of-sink accident (LOHS) and a LOHS without SCRAM (i.e., an anticipated transient without SCRAM or ATWS) scenarios. The first scenario generated a source term whereas the latter two sequences did not. The results from variations in some of the key reactor building performance parameters is also presented. A full Monte Carlo uncertainty analysis has been performed and will be reported separately from this paper. The base and sensitivity TOP scenarios are discussed in Sections 3.1 and 3.2, respectively. The LOHS and ATWS scenario results will be briefly discussed in Section 3.3. The discussion of the calculations includes the thermal-hydraulic

response of the reactor and the associated radionuclide release behavior.

## 3.1 Transient Overpower Scenario

The TOP scenario is initiated with a spurious rotation of  $B_4C$  arcs on the control drums away from the reactor core. The rotation of the control drums causes an increase in the reactivity. It is expected that the control drum position controller would have mechanical limitations to prevent a rapid rotation, which was assumed in this analysis. ORNL characterized the drum reactivity worth as a function of rotation angle. There is a 65-deg rotation from the  $k_{\text{eff}}=1$  drum position to a \$4.021 excess reactivity. Using this information, the maximum rotation speed of the rotation of 0.0016 deg/s was specified to yield a reactivity insertion rate of  $1x10^{-4}$  \$/s. This rotation speed generated a plausible response that would allow dynamic control during start-up and shutdown but a degree of safety from rapid changes.

The safety controls of the INL Design A were not described. A complete design would have a reactor protection system for the automatic emergency control rod insertion. The plant automatic emergency control rod shutdown system response is assumed to not operate in the TOP but the operators recognize the event and manually insert the controls rods after a time delay. The manual operation action was delayed until after the start of the fuel cladding failures (e.g., after high radiation signals). The scenario also assumes the trip of the secondary circulation system at the time of the manual SCRAM. Consequently, there is no active system heat removal.

### 3.1.1 TOP Reactor Response

The TOP reactor power response is shown Fig. 11. After an accelerated steady state calculation to establish the reactor reflector and radiation shield long-term temperature profile, the transient starts with a spurious rotation of the control drums. The increased reactivity leads to a power increase and a corresponding fuel and HP heatup. Due to the very strong negative reactivity with temperature (see Table 3), the increase in control drum reactivity is matched with a corresponding negative temperature reactivity feedback as the system temperature increases. The control drum reactivity addition and negative temperature feedback somewhat balance to yield a nearly linear power increase but with an associated fuel and HP temperature rise.

As indicated on a Fig. 11, the power increases from 5 MW to 8 MW over 0.9 hr when the highest power locations in the core reach the boiling limit. The core power drops due to additional negative feedback as portions of the core rapidly increase in temperature. The manual emergency control rod insertion is assumed to occur just after 1-hr.

The maximum fuel temperature response in Fig. 12 illustrates the linear temperature rise prior to boiling limit. The maximum fuel temperature location gradually heat-ups to 1300 K ( $\sim$ 1025°C). However, once the boiling limit occurs, the heat transfer to the HP fluid degrades and there is

a rapid local heatup of the fuel (i.e., similar to a transition from nucleate to film boiling in a water system above the critical heat flux). The cladding melts as the fuel passes the melting temperature of the stainless steel cladding, which starts the radionuclide release from the fuel. The HP is also assumed to fail and depressurize, which diminishes the heat transfer along the full length of the affected fuel assembly.

The manual emergency control rod insertion occurs just after 1-hr, which terminates the fission reaction. The secondary system is assumed to trip off at the same time, which stops all active heat removal. However, there is a strong passive heat dissipation away from the highest fuel temperature location thereafter. The fuel cooldown pauses near the melting temperature of the SS cladding as it refreezes and then continues cooling. The heat from the highest temperature regions near the center of the core steadily flows outward to the large surrounding reflector and radiation shield. As the outer vessel heats, a natural circulation of heated air leaving the reactor cavity to the first floor region is replaced by cooler air. The passive heat dissipation from the highest temperature fuel locations outward and the subsequent natural convection heat removal reduces the peak fuel location from 2200 K to 1200 K by 24 hr.

The response of the peak fuel location can be shown on the HP performance limit graph (see Fig. 13). As the HP power increases from the control drum reactivity insertion, the HP temperature increases. Once the HP reaches the boiling limit, the wall heat transfer decreases and the HP wall temperature rapidly increases, which causes the fuel cladding and HP wall failures. The trajectory of the power and temperature response is a function of the secondary heat removal characteristics due the close coupling between the fuel, the HP fluid temperature, and the HP wall temperature in the secondary condenser. As shown on the graph, only the boiling limit would be challenged in this scenario.

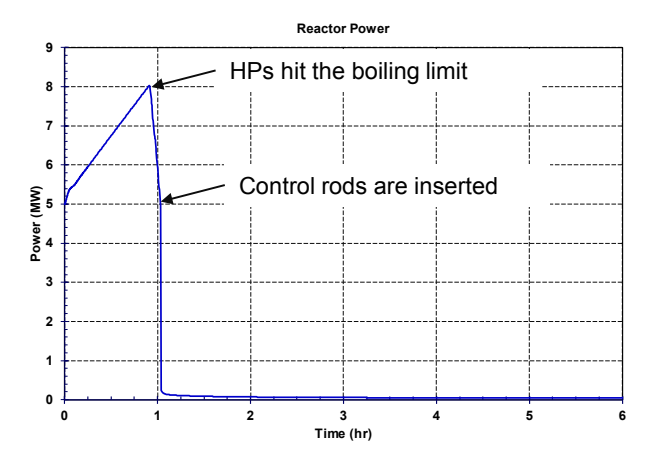


Fig. 11. Reactor power response in the TOP scenario.

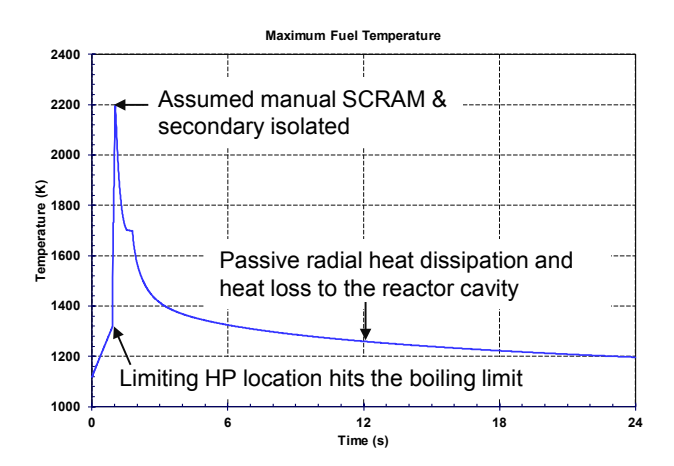


Fig. 12. Maximum fuel temperature response in the TOP scenario.

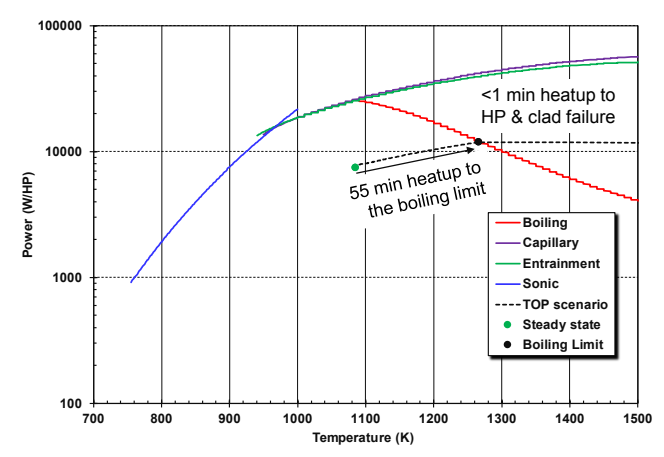


Fig. 13. TOP scenario response on the HP performance limit graph.

## 3.1.2 TOP Radionuclide Response

The pressure response of the failed heat pipes is shown in Fig. 14. Approximately 20% of the 1134 HPs failed. This corresponded to the 6 inner rings of the MELCOR core nodalization (i.e., Ring 2-7 on Fig. 9). When the HPs reached the boiling limit at the highest-powered location, the HP pressure and temperature dropped rapidly in response to the sudden reduction in heat addition but with the continued heat removal in the secondary. Consequently, the HPs failed closer to 2 bar rather than the peak value of up to 6 bar shown in Fig. 14.

The HP wall failed at the time of the fuel cladding failure, which provided a short-term motive force to push out any of the promptly releases fission products. Due to the very low fuel burnup, the initially mobile inventory in the gaps around the fuel is expected to be very small. Consequently, the HP blowdown had a relatively small impact on the initial radionuclide release. Furthermore, the relatively low peak

temperature (2200 K at the hottest fuel location) was followed by a prompt cooldown (see Fig. 12).

The iodine release from the fuel and its distribution is shown in Fig. 15. About 1.4% of the iodine inventory was released from the fuel. The assumed leak area from the vessel was 10.3 cm<sup>2</sup> (1.6 in<sup>2</sup>). However, there was relatively little motive force to discharge the iodine from the vessel into the reactor building. Furthermore, the release of iodine from the fuel diminished quickly following the reactor cooldown after the emergency control rod insertion. The long-term prediction was 89% of the released iodine remained in the vessel and only 11% in the reactor building or the environment.

The overall iodine release to the environment was 0.0008% of the total iodine fuel inventory. The leakage to the environment was affected by small assumed leak rate of 11.6 cm<sup>2</sup> (1.8 in<sup>2</sup>), the lack of a strong pressurization of the reactor building, and the dilution and settling in the reactor building prior to reaching the above grade leakage locations.

The leakage pathways active in the TOP scenario are shown in Fig. 16. The active pathways were the pathways from the cladding failure locations to the vessel leak location. The released radionuclides could bypass the reactor building if there was a creep rupture failure in the secondary side of the HP prior to the HP wall melt-through. The failed HP could be a more direct pathway from the core to the secondary side of the condenser via the HP with a failure location in the core and another in the condenser. In an open Brayton cycle, the secondary system discharges directly to the environment.

Fig. 17 and Fig. 18 show the intact and failed HP pressure responses and their associated creep failure index. If the creep rupture index reaches 1, then the HP is assumed to fail. The creep index has an exponential increase at high temperatures and pressures when the HP wall weakens. It is interesting to note that the HPs only reached a maximum of 6 bar prior to their melting failure whereas the remaining intact HPs reached much higher pressures (i.e., up to 13.5 bar) during the cooldown phase.

The maximum HP pressure and creep index occurred in the Ring 8, which was adjacent to the last ring with HP boiling limit transient and wall melt-through. A creep failure after the cooldown is not a risk of a direct pathway to the secondary and the environment because the HP would only have one failure location (i.e., two are needed for a flow pathway). Furthermore, a creep rupture failure cannot occur after a melt-through failure in the core because there is no driving pressure or temperature in the HP to further increase the creep. In summary, the creep index was too low for a creep failure (i.e., <1.e-6) when the boiling limit transient caused a wall melt-through.

Some exploratory variations showed it is very unlikely (i.e., not discovered in the exploratory runs) to have a HP creep failure prior to a boiling limit melt-through in the TOP scenario. Something like the trip of the secondary heat removal system was needed prior to reaching the boiling limit

and the subsequent manual emergency control rod shutdown. A secondary trip would allow the fuel and HP temperature to quickly rise at a lower HP power without a boiling limit heat transfer degradation. This was also more likely when the drum rotation rate was slowed and the manual shutdown action was further delayed. The additional scenario assumptions were judged unlikely but interesting to note for future probabilistic risk assessment evaluations.

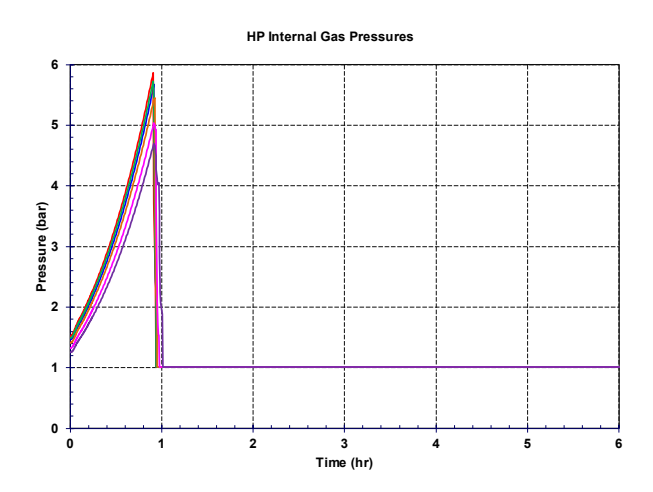


Fig. 14. Failed HP pressure response in the TOP scenario.

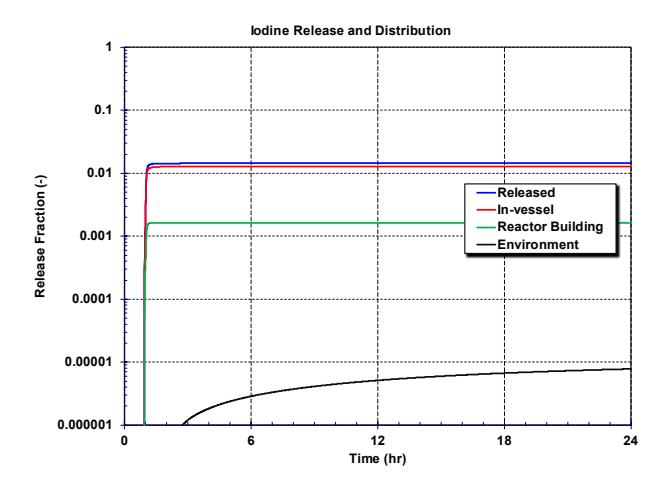


Fig. 15. Iodine release and distribution in the TOP scenario.

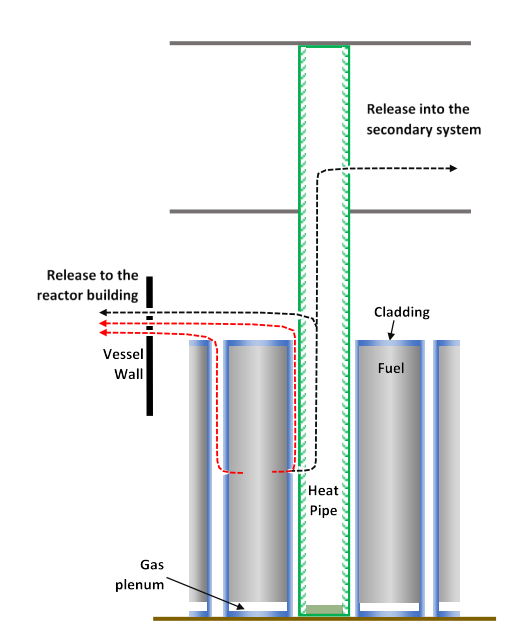


Fig. 16. Iodine release pathway in the TOP scenario.

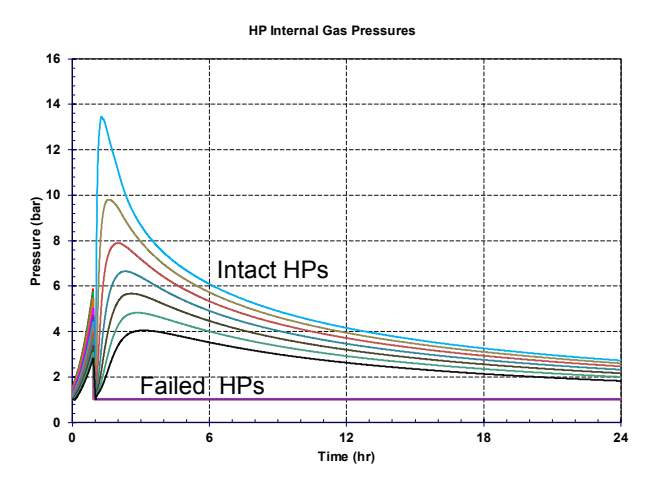


Fig. 17. The failed and intact HP pressure response in the TOP scenario.

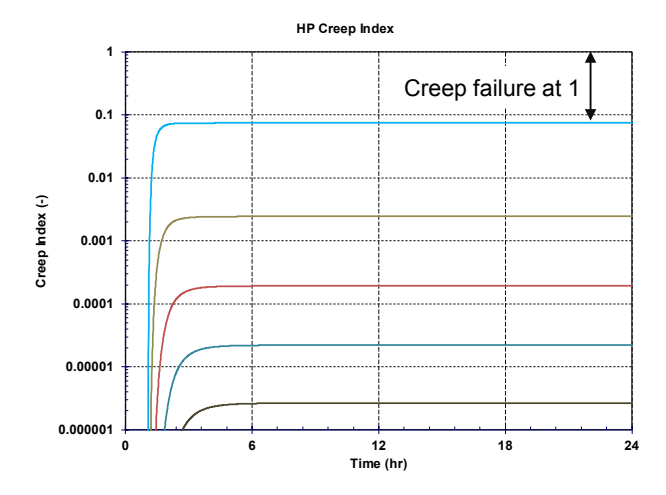


Fig. 18. HP creep rupture index in the TOP scenario.

## 3.2 Transient Overpower Scenario Sensitivity Calculations

MELCOR is well-suited for exploring calculational sensitivities. Many parameters in the physics routines can be easily sampled and varied using uncertainty sampling tools. In addition, MELCOR's building block format and control logic allows easy specification of the uncertain or variable boundary condition parameters. In anticipation of a full sensitivity study, a number of uncertain parameters were identified that were expected to impact the accident progression or the magnitude of the source term. The following examples varied one parameter at a time to their maximum and minimum values but subsequent studies will perform Monte Carlo uncertainty sampling of all parameters simultaneously.

The uncertain parameters and their sampling ranges in the TOP uncertainty study are shown in Fig. 19. The range of uncertain variables included the creep failure location (i.e., if any), the number of initially failed HPs (i.e., uniformly distributed across the core), the gaseous fraction of iodine, the control drum reactivity insertion rate, and the temperature feedback range. The effectiveness of the radiative heat transfer in the vessel, the vessel wall emissivity to the reactor cavity wall, the leakage area from the vessel to the reactor building, and the vessel heat transfer rate were uncertain parameters for the vessel thermal response. The reactor building uncertain parameters included a blockage fraction between the lower floor and the reactor cavity, the cavity wall emissivity, the external wind speed, and a multiplier to the building leakage rate. Finally, the timing of the response of the operator for a manual shutdown of the reactor was varied via the peak temperature in the core (i.e., as a surrogate for the timing of the action).

As an example of single variation of the uncertain parameters, the reactor building leakage rate and the external wind speed were selected. Fig. 20 shows the iodine release to the environment with variations in the building nominal leakage rate and the external wind speed.

The building leakage was scaled to a BWR reactor building (i.e., 11.6 cm² for 100%/day at 0.25 psi). A factor of 10X and 100X increased that value accordingly. While 100%/day is a seemingly large amount, this does not occur until the building over-pressurized to 1723 Pa (0.25 psi), or much, much larger than the building pressurization in the TOP scenario, which is negligible. For reference, a 100X building leakage (i.e., 0.116 m² or 180 in²) is equivalent to a 0.5 cm gap around a 6-m x 6-m equipment access door. Similarly, an external wind will increase the building infiltration and exfiltration. Wind effects are included in DOE nuclear facility analyses due to the low internal building driving forces for leakage.

The iodine environmental release results in Fig. 20 illustrate mechanisms that can reduce the reactor building retention. The solid blue line is the base response. As additional leakage and wind is added, the environmental release increases by a factor of 125 from  $8 \times 10^{-6}$  to  $\sim 10^{-3}$  with

100X leakage and a sustained wind speed of 10 mph. This example illustrates the sensitivity of the building leakage characteristics and environmental conditions on the magnitude of the overall source term.

Component	Parameter	Ranges
U Di	Heat Pipe Failure Location	Condenser (50%) / Evaporator (50%)
Heat Pipes	Initial non-functional HPs	0% - 5%
Core	Gaseous Iodine Fraction (-)	0.0 - 0.05
	Reactivity Insertion Rate (\$/s)	0.5x10 <sup>-4</sup> - 1.0x10 <sup>-3</sup>
	Total reactivity feedback	-0.0015 to -0.0025
Vessel	Fuel Element Radial View Factor Multiplier (-)	0.5 - 2.0
	Vessel Emissivity (-)	0.125 - 0.375
	Total Leak Area (m²)	2x10 <sup>-5</sup> - 2x10 <sup>-3</sup>
	Vessel and Vessel Upper Head HTC (W/m-K)	1 – 10
-		
Reactor Building	Cavity entrance open fraction	100% (90%) - 1% (10%)
	Cavity Emissivity (-)	0.125 - 0.375
	Wind Loading (m/s)	0 – 10
	Total Leak Area Multiplier (-)	1 - 100
Scenario	Peak fuel temperature for safety rod insertion	1300 – 2200 K

Fig. 19. Uncertain parameters in the TOP uncertainty calculations.

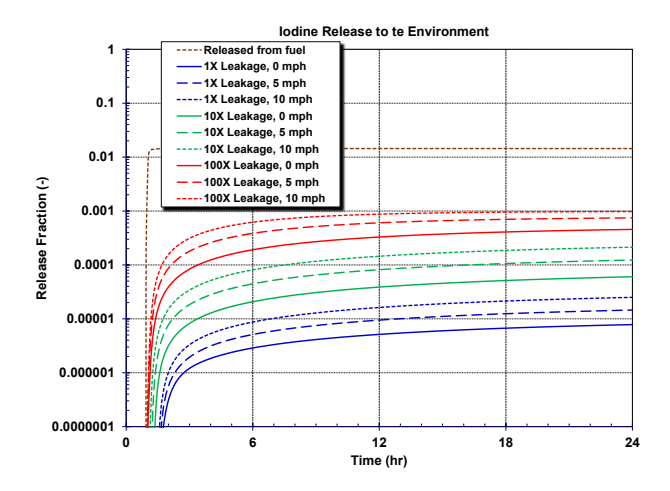


Fig. 20. Iodine release to the environment the TOP sensitivity calculations.

# 3.3 Loss-of-heat sink and ATWS

The loss-of-heat sink (LOHS) is another postulated scenario for HPR. In the LOHS scenario, the secondary heat removal trips off, which is followed by the actuation of the reactor shutdown system. There is no active heat removal. In a second variation, the reactor protection system is does not work, or an ATWS. Fig. 21 shows the peak fuel temperature for the two scenarios. Following the loss-of-heat removal, the temperature rises in both calculations but only reaches maximums of 911°C and 1036°C, respectively. Both peak temperatures show significant margin to a cladding failure. The responses are slightly different with the ATWS rising in temperature much more quickly whereas the LOHS has a slower response and a later peak fuel temperature.

The ATWS response includes a rapid temperature due to the additional fission power following the loss of heat removal. However, there are strong temperature negative reactivity feedback during the initial temperature rise. Fig. 22 shows the feedbacks going into the point kinetics model. The Doppler and fuel elongation is the dominant feedback with the radial expansion of the reflector and cladding as secondary effect. The fuel heats faster (i.e., average temperature rise of 159°C by 10 min versus 95°C for the reflector) and the feedback coefficient is larger (-0.00155 \$/°C versus -0.00064 \$/°C for the reflector, see Table 3). However, the net effect is a -0.31 \$ total reactivity insertion by 10 min due to the rapid temperature increase.

The associated power response is shown Fig. 23. Core power and decay heat in the ATWS.. The strong negative reactivity leads to a sharp decrease in the fission power from 4.66 MW to zero over 10 min. Consequently, the fission stopped and only the decay heat remains. A manual action to insert the control rods is credited to start the natural decrease in the decay heat. The decay heat decreases as predicted by the SCALE analysis thereafter. The long-term ATWS temperature is similar to the LOHS except the temperature offset due the initial temperature excursion.

The variation in the peak fuel temperature response to uncertain parameters (e.g., the ones in Fig. 19 for the TOP scenario) can be investigated to better understand the margins to success. This can be done through identification of key phenomena impacting the key figures of merit (e.g., the peak fuel temperature). However, the LOHS and ATWS examples illustrate other uses of MELCOR for probabilistic risk assessment success criteria in non-radionuclide release scenarios.

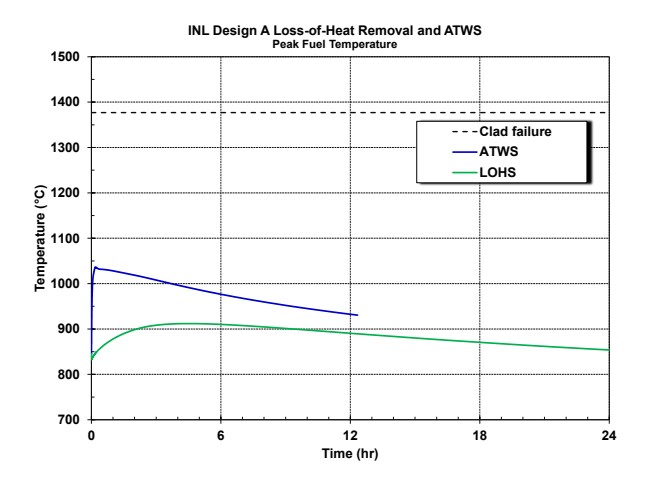


Fig. 21. Peak fuel temperature response in LOHS with and without emergency control rod insertion.

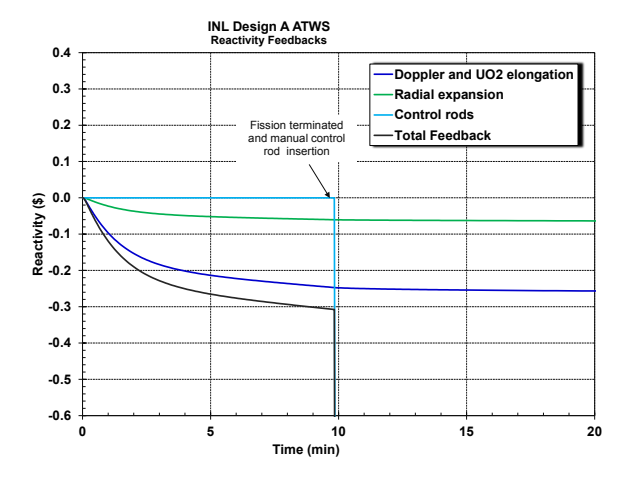


Fig. 22. Reactivity feedbacks in the ATWS.

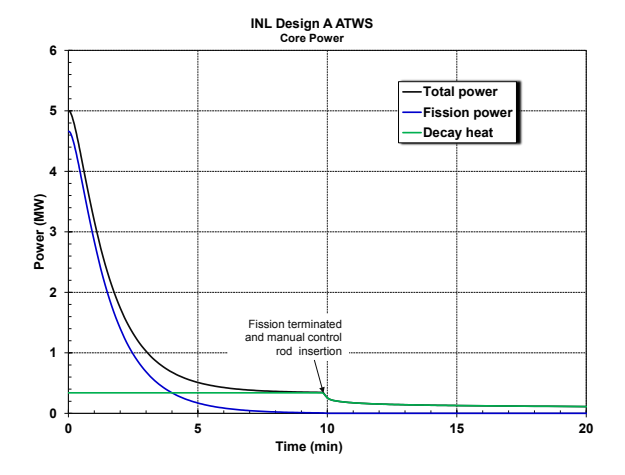


Fig. 23. Core power and decay heat in the ATWS.

## **SUMMARY**

The MELCOR code has been updated to support NRC evaluations of accidents in non-LWRs. This paper presents demonstration calculations for a HPR design from publicly available literature. A model of the INL Design A HPR was developed to demonstrate a mechanistic source term analysis, which included the heat pipe core, the secondary heat exchanger, and the reactor building. The HPR input model was used to demonstrate TOP, LOHS, and ATWS scenarios. The analyses demonstrate the flexible capabilities of MELCOR to evaluate the accident progression in an HPR. The code easily incorporates evolving data from ongoing research programs and includes flexible inputs for sensitivity and Monte Carlo sampling on uncertain parameters.

# **ACKNOWLEDGEMENTS**

This work was funded by the NRC Office of Nuclear Reactor Regulation as part of the development and demonstration activities defined in the NRC Non-Light Water Reactor Vision and Strategy Volume 3: Computer Code Development Plans for Severe Accident Progression, Source Term, and Consequence Analysis [3]. The authors gratefully acknowledge the contributions from Jason Schaperow, Hossein Esmaili, and Don Algoma of the US NRC for their valuable technical guidance.

Eric Walker and William Wieselquist of Oak Ridge National Laboratories performed the INL Design A SCALE analysis and provided the radionuclide decay heat power, the radionuclide inventory, the reactivity feedbacks, and the core axial and radial power profile for this analysis. The documentation of their analysis is forthcoming and part of the same NRC project [3].

Sandia National Laboratories is a multi-mission laboratory managed and operated by National Technology and Engineering Solutions of Sandia, LLC, a wholly owned subsidiary of Honeywell International, Inc., for the U.S. Department of Energy's National Nuclear Security Administration under contract DE-NA0003525.

The paper is archived at Sandia National Laboratories as SAND2021-XXXX.

### REFERENCES

- 1. MELCOR Computer Code Manuals: Volume 1; Primer and Users Guide Version 2.2.18019 Jan-2021.
- 2. MELCOR Computer Code Manuals: Volume 1; Reference Manual Version 2.2.18019 Jan-2021.
- 3. "Non-LWR Vision and Strategy Near-Term Implementation Action Plans," Nuclear Regulatory Commission, ADAMS Accession No. ML16334A495, 2019.
- 4. NASA, "Demonstration Proves Nuclear Fission System Can Provide Space Exploration Power,"
- https://www.nasa.gov/press-release/demonstration-proves-nuclear-fission-system-can-provide-space-exploration-power. May 2, 2018, Release 18-031.
- 5. MCCLURE, Patrick R., et al., "Design of Megawatt Power Level Heat Pipe Reactors," Los Alamos National Laboratory, 2015-11-12, LA-UR-15-28840, November 2015.
- 6. STERBENTZ, James W., et al., "Preliminary Assessment of Two Alternative Core Design Concepts for the Special Purpose Reactor," Idaho National Laboratory, INL/EXT-17-43212, Revision 1, May 2018.
- 7. WOLOSHUN, K. A., Merrigan, M. A., and Best, E. D., HTPIPE: A Steady-State Heat Pipe Analysis Program, A User's Manual," Los Alamos National Laboratory, LA-11324-M, November 1988
- 8. COTTER, T. P., "Theory of Heat Pipes," Los Alamos Scientific Laboratory, LA-3246-MS-UC-34, March 1965.
- 9. ANANTH, K. P., et al, "Portable Special Purpose Nuclear Reactor (2 MW) for Remote Operating Bases and Microgrids," 2017 Joint Service Power Expo, May 1-4, 2017, Virginia Beach, VA, INL/CON-17-41817.
- 10. WIESELQUIST, W. A., Lefebvre, R. A., and Jessee, M. A., Eds., "SCALE Code System," ORNL/TM-2005/39,

Version 6.2.4, Oak Ridge National Laboratory, Oak Ridge, TN (2020).

11. GAUNTT, R. O., "Synthesis of VERCOS and Phebus data in Severe Accident Codes and Applications," SAND2010-1633, Sandia National Laboratories, April 2010.